An ALE method for instabilities in the wake of multiple freely-oscillating bodies

Theo Mouyen, Javier Sierra Ausin, David Fabre, Flavio Giannetti

ERCOFTAC Symposium on "Multiphysics critical flow dynamics involving moving/ deformable structures with design applications", Toulouse, France, 7-8-9 June 2023

An ALE method for instabilities in the wake of multiple freely-oscillating bodies

Théo MOUYEN[1,2], Javier SIERRA-AUSÍN[1,2], David FABRE[1] and Flavio GIANNETTI[2]

[1] *IMFT, Institut de Mécanique des fluides de Toulouse, CNRS, Toulouse 31400, France*
[2] *Università degli Studi di Salerno - Via Giovanni Paolo II, 132, 84084 Fisciano, Italia*

Abstract.

Numerous current and future technological devices may benefit from the fundamental understanding of the fluid instabilities leading to Vortex Induced Vibrations (VIV). Energy harvesting devices are conceived to extract the mechanical energy of the flow by taking advantage of a fluid-structure instability that leads to a cyclic displacement of the structure. Herein, we propose a Linearised Eulerian-based Arbitrary Lagrangian Eulerian (L-ALE) method in order to rationalize the Eulerian and the Lagrangian character of the flow and structural variables, respectively. We first demonstrate that our method faithfully reproduces previous numerical results reported in the literature. Then, we study the flow configurations of $N = 2$ cylinders, in terms of the distinct fluid-structure instabilities and spatio-temporal properties of the global unstable modes.

Key words: instability, transition, cylinders, free-oscillations, VIV.

1 Introduction

Vortex induced vibrations (VIV) are of great interest to many fields of engineering. The design of structures that prevent such vibrations to avoid damage is an obvious example, cf [7]. One of their latest practical application worth mentioning is the design of submerged oscillating/deformable structures that are able to convert energy from marine currents and waves, e.g., the Wave Carpet [1] or VIVACE [2] projects. These applications aim, on the other hand, to optimize the structure displacement to allow increased energy harvesting.
The canonical case of a single freely-oscillating cylinder has been extensively studied with heavy focus on the lock-in phenomenon ([23]). It is defined as a synchronization between the the frequencies of the body's oscillation and of the vortex shedding. Outside of the lock-in regime, however, the frequency tends to the vortex shedding frequency of a fixed cylinder. [11] found that the lock-in phenomenon induces high amplitude movement of the cylinder, which are characterized by the absence of non-linear effects. It has also been shown that a decrease in the mass ration between body and fluid leads to a wider synchronization regime.
Configurations involving multiple cylinders have been scarcely explored. [3] directly simulated a tandem of cylinders for low reduced mass, $L/D = 1.5$ and $Re = 200$. For low reduced velocities, they found that the oscillation amplitudes are small therefore outside of the lock in region. The front cylinder exhibiting larger oscillation

amplitudes than the rear. An increase of the reduced velocity brings the cylinders' oscillations out of phase, increasing their amplitudes. At a critical reduced velocity, the cylinders continue to oscillate out of phase but the rear cylinder's amplitude becomes greater than the front one. The authors therefore found a wider lock-in region than for an isolated cylinder. Moreover, a structure that would be outside of the lock-in region can be brought in the lock in region by placing it in a tandem with a similar structure. This has important practical applications in the design of structures that need to prevent VIV. It is however a phenomenon that can be exploited for energy harvesting purposes. Thus, the VIVACE concept ([2]) converts ocean or river currents kinetic energy to electricity using vortex-induced vibrations of multiple oscillating cylinders. Nonetheless, the case of multiple cylinders has been mainly studied for fixed cylinders. Recently, [10] used an immersed boundary method to explore the flow past multiple rigidly-mounted cylinders. Depending on the distance separating the cylinders, three regimes exist. Increasing the spacing, the flow transitions from an attached regime to a fluctuating regime and finally to a vortex shedding regime. The fully attached regime is characterized by a steady flow in the gap between the cylinders whereas the fluctuating regime involves fluctuations in the gap. The vortex shedding regime on the other hand is characterized by vortex shedding in the gap, similar to that of a single cylinder's wake. For multiple cylinders, there is progression down the array from the attached to the fluctuating and in turn to the shedding regimes. For longer arrays of cylinders, this cascade repeats every few cylinder rows. On the other hand, the interaction between multiple freely-oscillating bodies has not been widely studied.
Hence, we propose a Linearised Arbitrary Lagrangian Eulerian method to explore the dynamics of multiple freely-oscillating bodies.

2 Numerical procedure

2.1 Problem formulation

We consider N spring-mounted cylinders immersed in a Newtonian fluid, with dynamic viscosity ν and density ρ. The cylinders have the densities ρ_n, spring stiffnesses k_n and damping parameters γ_n. Let $\tilde{\Omega}(t)$ denote the fluid domain and $\tilde{\Gamma}_n(t)$ its interface with the cylinders. The problem is governed by the following set of equations

$$\left.\frac{\partial \tilde{\boldsymbol{u}}}{\partial t}\right|_{\tilde{\boldsymbol{x}}} + (\tilde{\boldsymbol{\nabla}}\tilde{\boldsymbol{u}})\tilde{\boldsymbol{u}} - \tilde{\boldsymbol{\nabla}}\cdot\tilde{\boldsymbol{\sigma}}(\tilde{\boldsymbol{u}},\tilde{p}) = \boldsymbol{0} \qquad \text{in} \quad \tilde{\Omega}(t), \tag{1}$$

$$\tilde{\boldsymbol{\nabla}}\cdot\tilde{\boldsymbol{u}} = 0 \qquad \text{in} \quad \tilde{\Omega}(t), \tag{2}$$

$$\ddot{y}_n + \frac{4\pi\gamma_n}{U_n^*}\dot{y}_n + \left(\frac{2\pi}{U_n^*}\right)^2 y_n = \frac{2C_{y_n}(t)}{\pi m_n^*}, \tag{3}$$

$$\dot{y}_n = \tilde{u} \qquad \text{on} \quad \tilde{\Gamma}_n(t). \tag{4}$$

In eqs. (1) to (4), the symbol ($\tilde{}$) is used for time dependant quantities as well as time and spacial derivatives evaluated in the time dependant domain. The stress tensor is defined as $\tilde{\boldsymbol{\sigma}}(\tilde{\boldsymbol{u}},\tilde{p}) = -\tilde{p}\mathbf{I} + \frac{1}{Re}\left(\tilde{\boldsymbol{\nabla}}\tilde{\boldsymbol{u}} + \tilde{\boldsymbol{\nabla}}\tilde{\boldsymbol{u}}^{\mathrm{T}}\right)$ where the Reynolds number

$Re = \frac{U_\infty D}{\nu}$ is defined using as a reference length and velocity the diameter of the cylinders D and the uniform velocity at the far field. In the previous expressions, the index n is used to refer to the n^{th} cylinder, see fig. 1. $C_{y_n}(t)$ is the vertical force coefficient and m_n^* the mass ratio between the cylinder and fluid densities. The reduced velocity is referred to as $U_n^* = 2\pi U_\infty \sqrt{m_{c_n}/k_n/D}$, where m_{c_n} and k_n are the n^{th} cylinder's mass and spring stiffness.

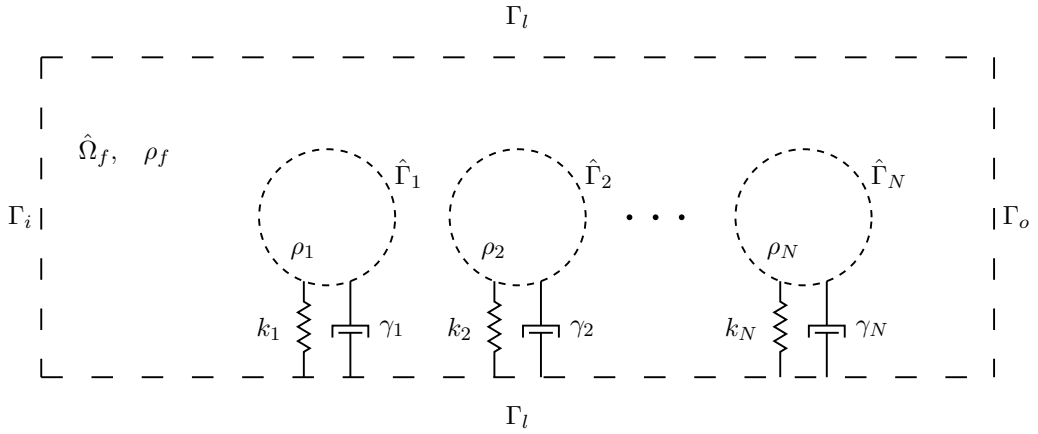

Figure 1: Array of N spring mounted cylinders with densities, spring stiffness and damping parameters: ρ_n, k_n and γ_n. The cylinders are immersed in a fluid domain $\hat{\Omega}_f$ of density ρ_f. The domain is delimited by inlet and outlet boundaries, Γ_i and Γ_o as well as lateral boundaries Γ_l.

2.2 ALE formulation

The Arbitrary Lagrangian Eulerian method is a conforming method that allows to treat interfaces in a Lagrangian frame of reference while the fluid is treated in an Eulerian frame of reference. We consider a fixed reference domain $\hat{\Omega}$ where unknowns are evaluated in an Eulerian frame of reference. Lagrangian variables on the other hand are evaluated on the actual physical domain $\tilde{\Omega}(t)$, which is time dependant. Let us define the diffeomorphism $\mathcal{A}$ that allows us to express the position $\tilde{\boldsymbol{x}}(t)$ of the actual domain with respect to the position $\hat{\boldsymbol{x}}$ of the reference domain:

$$\begin{aligned} \mathcal{A} : \hat{\Omega} \times \mathbb{R}^+ &\longrightarrow \tilde{\Omega} \times \mathbb{R}^+ \\ (\hat{\boldsymbol{x}}, t) &\longmapsto (\tilde{\boldsymbol{x}}(t), t) \end{aligned} \tag{5}$$

This diffeomorphism allows a mapping of the actual domain through the position

$$\tilde{\boldsymbol{x}} = \hat{\boldsymbol{x}} + \hat{\boldsymbol{\xi}}_e(\hat{\boldsymbol{x}}, t) \tag{6}$$

where $\hat{\boldsymbol{\xi}}_e$ is an extension displacement field that propagates the Lagrangian interface deformation to the rest of the domain. This field is arbitrary and usually dictated by an elliptic equation $-\hat{\nabla} \cdot \boldsymbol{\Sigma}_e \left(\hat{\boldsymbol{\xi}}_e \right) = \mathbf{0}$ that ensures a smooth distribution over the whole domain. Following the method used by [13, 18], we apply the diffeomorphism to the Lagrangian variables in eqs. (1) and (2) which yields the non-conservative ALE formulation of the incompressible Navier-Stokes equation:

$$\hat{J}\left(\hat{\boldsymbol{\xi}}_e\right)\frac{\partial\hat{\boldsymbol{u}}}{\partial t}+\left(\hat{\boldsymbol{\nabla}}\hat{\boldsymbol{u}}\hat{\Phi}\left(\hat{\boldsymbol{\xi}}_e\right)\right)\left(\hat{\boldsymbol{u}}-\frac{\partial\hat{\boldsymbol{\xi}}_e}{\partial t}\right)-\hat{\boldsymbol{\nabla}}\cdot\hat{\boldsymbol{\Sigma}}\left(\hat{\boldsymbol{u}},\hat{p},\hat{\boldsymbol{\xi}}_e\right)=\mathbf{0}\quad\text{in}\quad\hat{\Omega}\tag{7}$$

$$-\hat{\nabla}\cdot\boldsymbol{\Sigma}_e\left(\hat{\boldsymbol{\xi}}_e\right)=\mathbf{0}\quad\text{in}\quad\hat{\Omega}\tag{8}$$

$$-\hat{\boldsymbol{\nabla}}\cdot\left(\hat{\boldsymbol{\Phi}}\left(\hat{\boldsymbol{\xi}}_e\right)\hat{\boldsymbol{u}}\right)=0\quad\text{in}\quad\hat{\Omega}\tag{9}$$

In the previous expression, $\hat{\boldsymbol{\Phi}}\left(\hat{\boldsymbol{\xi}}_{\mathrm{e}}\right)=\hat{J}\left(\hat{\boldsymbol{\xi}}_{\mathrm{e}}\right)\hat{\mathbf{F}}\left(\hat{\boldsymbol{\xi}}_{\mathrm{e}}\right)^{-1}$ is a deformation operator introduced by the variable change, with $\hat{J}\left(\hat{\boldsymbol{\xi}}_{\mathrm{e}}\right)=\det\left(\hat{\mathbf{F}}\left(\hat{\boldsymbol{\xi}}_{\mathrm{e}}\right)\right)$ the Jacobian of the deformation gradient $\hat{\mathbf{F}}\left(\hat{\boldsymbol{\xi}}_{\mathrm{e}}\right)=\mathbf{I}+\hat{\boldsymbol{\nabla}}\hat{\boldsymbol{\xi}}_{\mathrm{e}}$. The ALE fluid stress tensor expressed in the reference configuration writes as

$$\hat{\boldsymbol{\Sigma}}\left(\hat{\boldsymbol{u}},\hat{p},\hat{\boldsymbol{\xi}}_{\mathrm{e}}\right)=\hat{\boldsymbol{\sigma}}\left(\hat{\boldsymbol{u}},\hat{p},\hat{\boldsymbol{\xi}}_{\mathrm{e}}\right)\hat{\boldsymbol{\Phi}}\left(\hat{\boldsymbol{\xi}}_{\mathrm{e}}\right)^{\mathrm{T}}\tag{10}$$

with the viscous dissipation tensor

$$\hat{\mathbf{D}}\left(\hat{\boldsymbol{u}},\hat{\boldsymbol{\xi}}_{\mathrm{e}}\right)=\frac{1}{2}\frac{1}{\hat{J}\left(\hat{\boldsymbol{\xi}}_{\mathrm{e}}\right)}\left((\hat{\boldsymbol{\nabla}}\hat{\boldsymbol{u}})\hat{\boldsymbol{\Phi}}\left(\hat{\boldsymbol{\xi}}_{\mathrm{e}}\right)+\hat{\boldsymbol{\Phi}}\left(\hat{\boldsymbol{\xi}}_{\mathrm{e}}\right)^{\mathrm{T}}(\hat{\boldsymbol{\nabla}}\hat{\boldsymbol{u}})^{\mathrm{T}}\right).\tag{11}$$

Hereinafter, we particularize the elliptic operator $\boldsymbol{\Sigma}_e=\nabla$, that is, the extension displacement field is determined by solving a Laplace equation. The complete formulation used to determine the extension field is as follows,

$$\begin{cases}\Delta\hat{\boldsymbol{\xi}}_e=\mathbf{0} & (12)\\ \hat{\boldsymbol{\xi}}_{e_{\Gamma_i}}=y_i\quad\text{on}\quad\Gamma_i & (13)\\ \hat{\boldsymbol{\xi}}_{e_{\Gamma_j}}=0\quad\text{on}\quad\Gamma_{j,i}\neq j. & (14)\end{cases}$$

The eq. (12) is linear, and the number of cylinders is finite, thus we can look for a solution of the extension field as a function of the cylinders' vertical displacement:

$$\hat{\boldsymbol{\xi}}_e=\sum_{i=1}^{N}y_i\hat{\boldsymbol{\xi}}_{e_i}.\tag{15}$$

The extension field is therefore decoupled from the system and can be calculated a priori.

2.3 Linearised-ALE (L-ALE) for VIV problems

In the following, we detail the procedure employed to analyse the asymptotic stability of the fluid-structure configuration. First, we write the FSI variable $\hat{\boldsymbol{q}}=\left(\hat{\boldsymbol{u}},\hat{p},\hat{\boldsymbol{\xi}}_e,y_1,...,y_n,z_1,...,z_n\right)$. Then, we decompose the flow field into

$$\hat{\boldsymbol{q}}(\hat{\boldsymbol{x}},t)=\hat{\boldsymbol{q}}_0(\hat{\boldsymbol{x}})+\varepsilon\hat{\boldsymbol{q}}'(\hat{\boldsymbol{x}},t),\tag{16}$$

where $\hat{\boldsymbol{q}}'$ is a perturbation about the base flow $\hat{\boldsymbol{q}}_0$, and $\varepsilon\ll 1$. Substituting the ansatz eq. (16) into eqs. (1) to (4) and taking the Laplace transform of the time variable leads to the following formulations. In the following, we will denote by $\boldsymbol{q}$ the Laplace transform of $\hat{\boldsymbol{q}}'$.

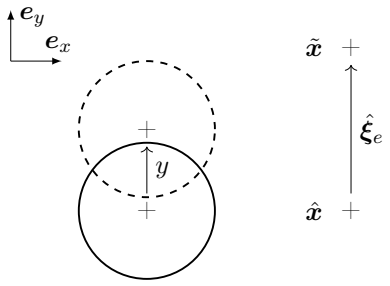

Figure 2: Sketch of the geometrical transformations involved in the ALE approach.

ALE fluid-structure coupled formulation

$$\lambda \left(\underbrace{\boldsymbol{u}}_{B_0} - \underbrace{\sum_{i=1}^{N} y_i \boldsymbol{\xi}_i \cdot \nabla_0 \hat{\boldsymbol{u}}_0}_{B_i} \right) = \underbrace{-\left((\nabla_0 \hat{\boldsymbol{u}}_0)\boldsymbol{u} + (\nabla_0 \boldsymbol{u})\hat{\boldsymbol{u}}_0\right) - \nabla_0 p + 2\mu \nabla_0 \cdot \boldsymbol{D}(\boldsymbol{u})}_{A_0}$$
$$+ \sum_{i=1}^{N} y_i \Bigg[- \nabla_0 \hat{\boldsymbol{u}}_0 \big(\nabla_0 \cdot \boldsymbol{\xi}_i I - \nabla_0 \boldsymbol{\xi}_i\big)\hat{\boldsymbol{u}}_0 - \nabla_0 \cdot \hat{p}_0 \big(\nabla_0 \cdot \boldsymbol{\xi}_i I - \nabla_0 \boldsymbol{\xi}_i\big)$$
$$\underbrace{-\mu \nabla_0 \cdot \Big(\nabla_0 \hat{\boldsymbol{u}}_0 \nabla_0 \boldsymbol{\xi}_i + (\nabla_0 \boldsymbol{\xi}_i)^T (\nabla_0 \hat{\boldsymbol{u}}_0)^T\Big) + 2\mu \nabla_0 \cdot \Big(\boldsymbol{D}_0(\hat{\boldsymbol{u}}_0)\big(\nabla_0 \cdot \boldsymbol{\xi}_i I - \nabla_0 \boldsymbol{\xi}_i\big)\Big)}_{A_i} \Bigg], \tag{17}$$

$$0 = \underbrace{\nabla_0 \boldsymbol{u}}_{D_0} + \sum_{i=1}^{N} y_i \underbrace{\nabla_0 \cdot \Big(\big(\nabla_0 \cdot \boldsymbol{\xi}_i I - \nabla_0 \boldsymbol{\xi}_i\big)\hat{\boldsymbol{u}}_0\Big)}_{D_i}. \tag{18}$$

The linearization of eqs. (7) and (9) introduces the terms A_0 and D_0 that are purely driven by fluid variables, and the terms A_i and D_i that arise from the interaction of fluid and ALE variables.

Cylinders equations Defining $z_i = \dfrac{\partial y_i}{\partial t}$ as the velocity of a cylinder, and introducing eq. (16) in eq. (3), we obtain the following system for each cylinder

$$\lambda y = z_i, \tag{19}$$

$$\lambda z_i = -\Gamma_i z_i - \Omega_i y_i + C_i + \tilde{C}_i(y). \tag{20}$$

The vertical force acting on each cylinder can be divided in two components. The first one is found by integrating on the boundary the stress which is purely linked to the fluid motion:

$$C_i = \frac{4}{\pi m^*} \int_{\Gamma_i} \big(- p\boldsymbol{I}\boldsymbol{n} + 2\mu \boldsymbol{D}_0(\boldsymbol{u})\boldsymbol{n}\big) \cdot \boldsymbol{e}_{y_i} \, d\Gamma_i. \tag{21}$$

In eq. (17), part of the stress results in a coupling of the fluid variables with the extension field, which after integration leads to the second lift component:

$$\tilde{C}_i(y_j) = \sum_{j=1}^{N} y_j \Big(\frac{4}{\pi m^*} \int_{\Gamma_j} \big(\quad (-\hat{p}_0 \boldsymbol{I} + 2\mu \boldsymbol{D}_0(\hat{\boldsymbol{u}}_0)) \left(\nabla_0 \cdot \boldsymbol{\xi}_j I - \nabla_0 \boldsymbol{\xi}_j\right)^T \\ -\mu \left(\nabla_0 \hat{\boldsymbol{u}}_0 \nabla_0 \boldsymbol{\xi}_j + (\nabla_0 \boldsymbol{\xi}_j)^T (\nabla_0 \hat{\boldsymbol{u}}_0)^T\right) \big) \boldsymbol{n} \cdot \boldsymbol{e}_{y_j} \, d\Gamma_j \Big).$$

Matricial system The system of equations described above can therefore be written as the following matricial system

$$\lambda \boldsymbol{B} \boldsymbol{q} = \boldsymbol{A} \boldsymbol{q}, \tag{22}$$

with matrices

$$\boldsymbol{B} = \begin{bmatrix} B_0 & B_1 & \dots & B_N & 0 & \dots & 0 \\ 0 & 0 & \dots & 0 & 0 & \dots & 0 \\ & I_d & & & & & \\ & & \ddots & & & (0) & \\ & & & I_d & & & \\ & & & & I_d & & \\ & (0) & & & & \ddots & \\ & & & & & & I_d \end{bmatrix} \tag{23}$$

and

$$\boldsymbol{A} = \begin{bmatrix} A_0 & A_1 & \dots & A_N & 0 & \dots & 0 \\ D_0 & D_1 & \dots & D_N & 0 & \dots & 0 \\ & & & & I_d & & \\ & & (0) & & & \ddots & \\ & & & & & & I_d \\ C_1 & \tilde{C}_1(y_1) - \Omega_1 & & \tilde{C}_1(y_N) & -\Gamma_1 & & \\ \vdots & \vdots & \ddots & \vdots & & \ddots & \\ C_N & \tilde{C}_N(y_1) & & \tilde{C}_N(y_N) - \Omega_N & & & -\Gamma_N \end{bmatrix}. \tag{24}$$

Equation 22 is rewritten in a variational formulation, spacially discretised and solved with the FreeFem++ software ([8]). The system is complemented with suitable boundary conditions for the external boundaries (Γ_i, Γ_l, Γ_o). A Dirichlet boundary condition is imposed at the inflow boundary Γ_i: $\hat{\boldsymbol{u}}_0|_{\Gamma_i} = U_\infty$, $\boldsymbol{u}|_{\Gamma_i} = 0$, and a stress-free condition is imposed on the lateral and outflow boundaries. Additionally, to the linearised problem, we employ the complex mapping method ([15, 20]) to faithfully characterise the stability properties of the problem and to suppress artificial unstable modes arising due to a non-local feedback between the outflow boundary and the near-wake. Such a method has been successfully employed in the past in other fluid configurations, for instance, the jet flow past a circular aperture [16, 9], a flow configuration of two coaxial jets [5] or wake flow past a rotating particle [17]. When using the complex mapping method, the spatial structure of the global mode near the boundary becomes evanescent and do not have an influence on the stability properties of the problem.

2.4 Validation

The L-ALE code is validated against the canonical cases of one fixed cylinder as well as one freely-oscillating cylinder. By setting $U_1^* = m_1^* = \infty$ in eq. (3), we investigate the stability of the flow around a fixed cylinder. At critical Reynolds number of 47, the first mode becomes unstable as can be seen in figure 3. We then

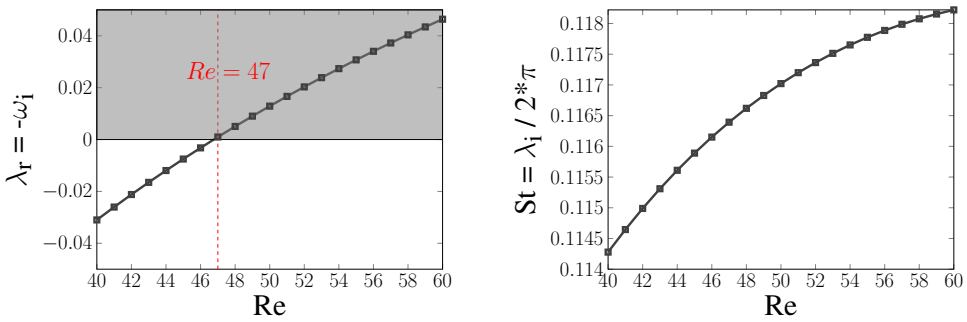

Figure 3: Growth rate and Strouhal number of the leading mode in the case of a fixed cylinder. Present results are shown as — and compared to results produced from the code developed by [6] (▣).

set the damping ratio γ to zero and vary the reduced velocity U^* at the two reduced masses $m^* = \{5, 20\}$ for a fixed Reynolds number of $Re = 60$. According to [11] and [14], two leading unstable modes are found. These modes are referred to as the elastic mode (EM) and the fluid mode (FM). Figure 4 shows the real and imaginary parts of both eigenvalues as a function of U^* for $Re = 60$ and $m^* = \{5, 20\}$. The eigenvalue of the EM mode tends to the natural structural frequency of the cylinder, whereas the eigenvalue of the FM mode is similar to the one of the fixed cylinder case. Overall, the L-ALE method developed for the present study shows consistent results compared to data from [14]. We found qualitative agreement against the results reported by [22]. A possible explanation of the quantitative discrepancy found for reduced velocities higher than $U^* = 6$ could be the use of a coarse mesh or small added mass effects that emerge for large U^* or small m^*. Further investigation on the reasons for this disagreement will be presented during the conference.

3 Results and discussion

We investigate the flow dynamics and interaction with two elastically mounted cylinders of the same reduced mass $m^* = 2.546$. Throughout this study, the damping parameter of both cylinders is set to zero. Within the range of Reynolds numbers $Re < 200$, there are three unstable global modes. Figures 5(a) and 5(c) show the real and imaginary parts of the eigenvalues against U^* for $Re = 100$ and $m^* = 2.546$. These results are also compared with data from [22]. The structure of the modes is shown in figure 6. For value of reduced mass $m^* = 2.546$, the structure of the third mode (—) resembles the one of the wake of two fixed cylinders (figure 6(e)). Its frequency remains constant and is slightly higher compared to the frequency of the leading mode behind the fixed cylinder tandem $\omega_f = 0.76$ (···). It therefore appears to be a purely fluidic mode and will be named FM. Modes 1 and 2 seem however to have a more complex structure arising from the fluid structure interac-

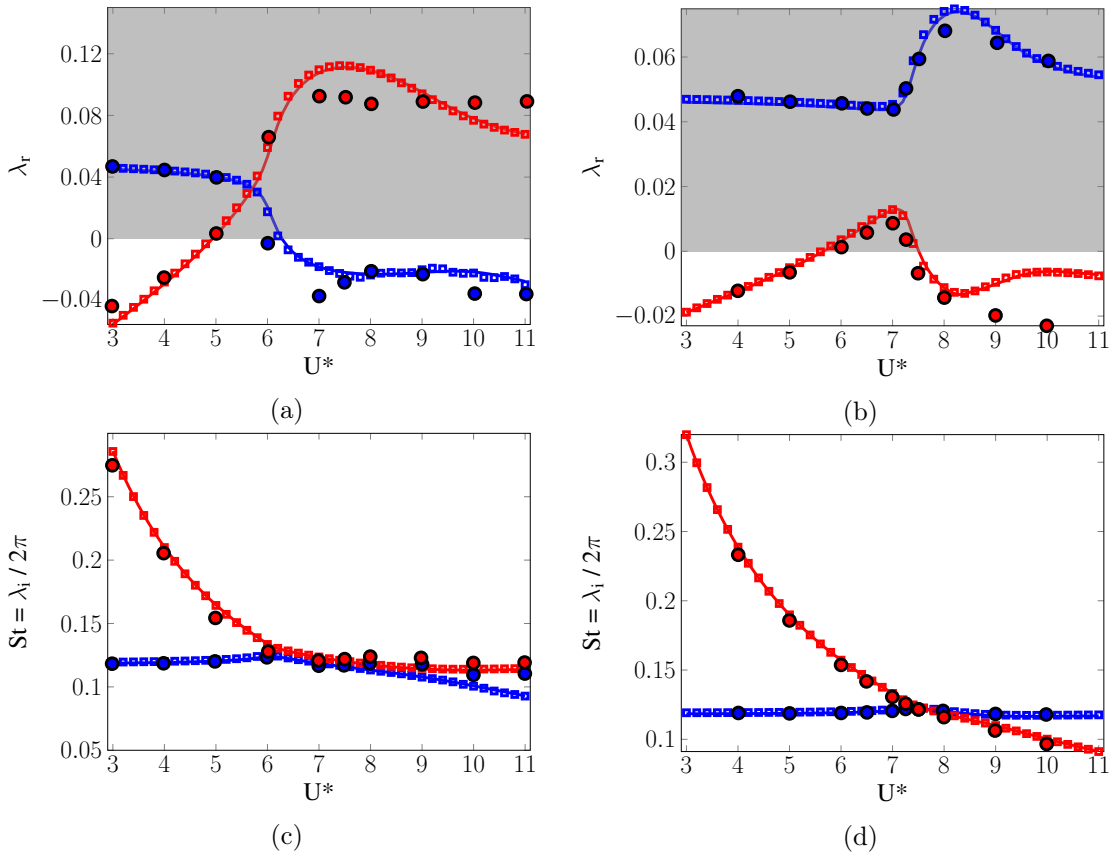

Figure 4: Real and imaginary parts of the leading eigenvalues with respect to U^* at $Re = 60$ for $m^* = 5$ (a,c) and $m^* = 20$ (b,d). The unstable region is depicted as the grey zone. The eigenvalues of the two leading modes found by the present study are respectively shown by —, —. Results found by [14] are displayed as □ and □; and results from [22] are shown as ● and ●.

tion. They will be respectively named as FEMI (—) and FEMII (—), following the denomination used by [11]. For low reduced velocities, FMI matches the natural frequency of a cylinder ($\omega_n = \frac{2\pi}{U_n^*}$, shown as - -), and the mode remains stable. For higher reduced velocities, the mode becomes unstable and its frequency tends to ω_f but the two cylinders display transverse motion, confirming the structural nature of the mode (figure 6(a)). On the other hand, FEMII frequency's mayches ω_f for low reduced velocities and remains stable. For moderate to higher reduced velocities, the mode becomes unstable and its frequency decreases. Transverse motion of the two cylinders is present, again showing the structural nature of the mode.

For $m^* = 20$, the transverse motion of the two cylinders introduces four unstable complex-conjugate eigenvalues and associated eigenmodes. Figures 5(b) and 5(d) show the real and imaginary parts of the eigenvalues against U^* for $Re = 100$ and $m^* = 20$. The FM (—),FEMI (—) and FEMII (—) modes are still present at $m^* = 20$. FM however remains stable for all reduced velocities invistigated. The frequency of FEMII has a similar behaviour to that at $m^* = 2.546$. It matches the fixed tandem case up to a reduced veloctity of $U^* = 7.5$ and then starts decreasing. Its growth rate however shows that the mode is unstable over most of the range of reduced velocities explored. Only around $U^* = 7.5$ is the mode stable. The

frequency of FEMII matches ω_n up to a reduced velocity of $U^* = 7.5$, after witch it tends to ω_f. An additional unstable mode is found for $m^* = 20$. Its behaviour and structure show similarities to FEMII, we will call it FEMIII (—). Where FEMII is unstable for all reduced velocities greater than $U *^{=} 4$, FEMIII is only unstable around $U^* = 4$ an $U^* = 7.5$.
The behaviour of the modes around $U^* = 7.5$ lead us to believe in the existence of a complex non-linear bearing. We will further explore that region by the means of weakly non-linear methods as well as direct numerical simulations.

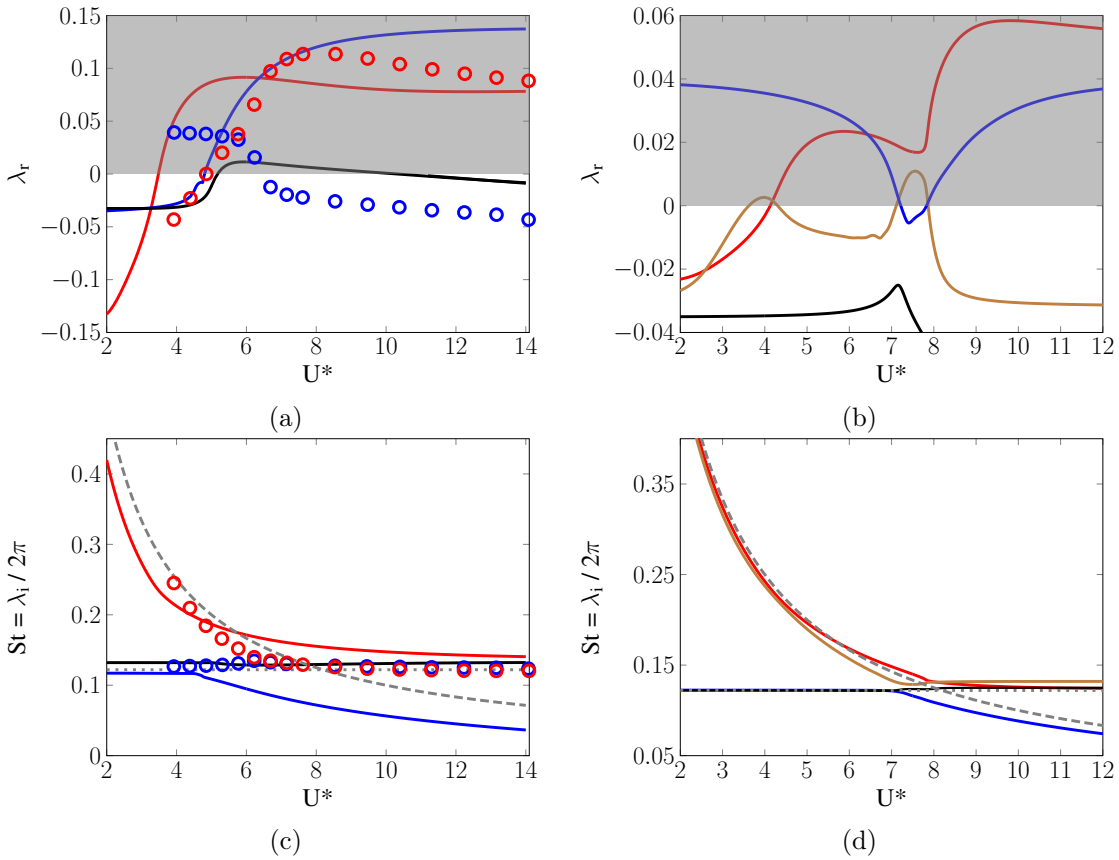

Figure 5: Real and imaginary parts of the leading eigenvalues with respect to U^* at $Re = 100$ for $m^* = 2.546$ (a,c) and $m^* = 20$ (b,d). The unstable region is depicted as the grey zone. The eigenvalues of the three leading modes found by the present study are shown by —, — and —. Results from [22] are shown by ○ and ○. The natural frequency of the cylinders $\omega_n = \frac{2\pi}{U_n^*}$ is shown as – –. The frequency of the fluid mode behind two fixed cylinders ($\omega_f = 0.76$) is displayed as · · ·.

4 Conclusion & perspectives

We propose a Linearised Arbitrary Lagrangian Eulerian method to study the Vortex Induced Vibrations of multiple bodies. The method was derived in order to decouple the field associated with mesh deformation from the other unknowns of the problem, hence considerably decreasing computational time. The outcome of linear stability analysis of a single freely-oscillating cylinder showed good accordance with results

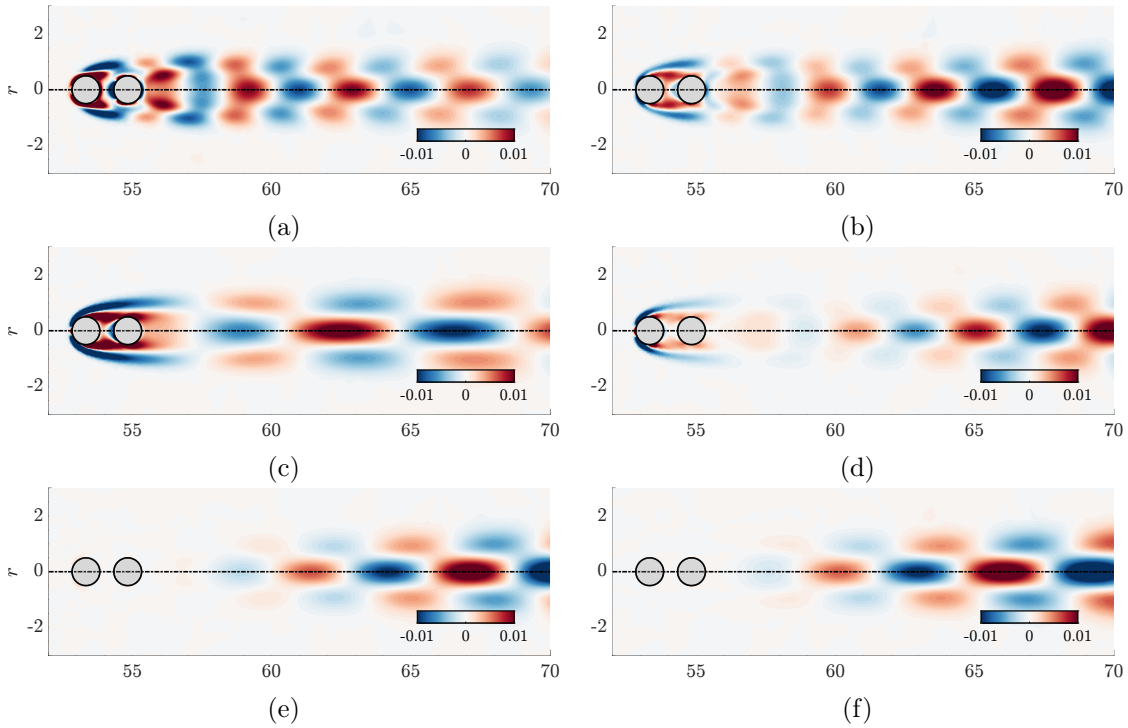

Figure 6: Vorticity of the three leading modes at $Re = 100$ and $U^* = 6$ for a reduced mass of $m^* = 2.546$ (a,c,e) and of $m^* = 20$ (b,d,f): FEMI (a,b), FEMII (c,d) and FM (e,f).

from the literature. The method was then applied to a tandem of freely-oscillating cylinders. The structure and behaviour of the leading eigenmodes was described for a set of reduced masses at fixed Reynolds number.
Nonlinear effects will be considered in future studies. In particular, we aim to develop an efficient time-stepping Finite Element solver [4], similar to the one developed in the thesis of Pfister [12]. In a second step, we would like to continue the limit cycles emerging from the Hopf bifurcations highlighted herein. To do so, we would like to reconstruct the limit cycle with the Harmonic Balance method [19], and to determine the existence of secondary instabilities with the Floquet-Hill technique [21].

References

[1] Mohammad-Reza Alam. Nonlinear analysis of an actuated seafloor-mounted carpet for a high-performance wave energy extraction. *Proceedings of the Royal Society A: Mathematical, Physical and Engineering Sciences*, 468(2146):3153–3171, 2012.

[2] Michael M Bernitsas, Kamaldev Raghavan, Y Ben-Simon, and EMH Garcia. Vivace (vortex induced vibration aquatic clean energy): A new concept in generation of clean and renewable energy from fluid flow. *Journal of offshore mechanics and Arctic engineering*, 130(4), 2008.

[3] Iman Borazjani and Fotis Sotiropoulos. Vortex-induced vibrations of two cylinders in tandem arrangement in the proximity–wake interference region. *Journal of fluid mechanics*, 621:321–364, 2009.

[4] V Citro, F Giannetti, and J. Sierra-Ausin. Optimal explicit runge-kutta methods for compressible navier-stokes equations. *Applied Numerical Mathematics*, 152:511–526, 2020.

[5] A. Corrochano, J. . Sierra-Ausin, J. A. Martin, D. Fabre, and S. Le Clainche. Mode selection in concentric jets: the steady-steady 1:2 resonant mode interaction with o(2) symmetry. *Journal of Fluid Mechanics*, 2023.

[6] David Fabre, Vincenzo Citro, D Ferreira Sabino, Paul Bonnefis, Javier Sierra, Flavio Giannetti, and Maxime Pigou. A practical review on linear and nonlinear global approaches to flow instabilities. *Applied Mechanics Reviews*, 70(6), 2018.

[7] OM Griffin and SE Ramberg. Some recent studies of vortex shedding with application to marine tubulars and risers. 1982.

[8] Frédéric Hecht. New development in freefem++. *Journal of numerical mathematics*, 20(3-4):251–266, 2012.

[9] Lionel Hirschberg, Juan G Guzman Inigo, Alessia Aulitto, Sierra-Ausin, Javier, David Fabre, Aimee Morgans, and A Hirschberg. Linear theory and experiments for laminar bias flow impedance: Orifice shape effect. page 2887, 2022.

[10] N Hosseini, MD Griffith, and JS Leontini. The flow past large numbers of cylinders in tandem. *Journal of Fluids and Structures*, 98:103103, 2020.

[11] Sanjay Mittal et al. Lock-in in vortex-induced vibration. *Journal of Fluid Mechanics*, 794:565–594, 2016.

[12] Jean-Lou Pfister. *Instabilities and optimization of elastic structures interacting with laminar flows*. PhD thesis, Université Paris-Saclay, 2019.

[13] Jean-Lou Pfister, Olivier Marquet, and Marco Carini. Linear stability analysis of strongly coupled fluid–structure problems with the arbitrary-lagrangian–eulerian method. *Computer Methods in Applied Mechanics and Engineering*, 355:663–689, 2019.

[14] Diogo Sabino, David Fabre, JS Leontini, and D Lo Jacono. Vortex-induced vibration prediction via an impedance criterion. *Journal of Fluid Mechanics*, 890, 2020.

[15] Javier Sierra, David Fabre, and Vincenzo Citro. Efficient stability analysis of fluid flows using complex mapping techniques. *Computer Physics Communications*, 251:107100, 2020.

[16] J. Sierra-Ausin, D Fabre, V Citro, and F Giannetti. Acoustic instability prediction of the flow through a circular aperture in a thick plate via an impedance criterion. *Journal of Fluid Mechanics*, 943, 2022.

[17] J Sierra-Ausin, M Lorite-Diez, JI Jimenez-Gonzalez, V Citro, and D Fabre. Unveiling the competitive role of global modes in the pattern formation of rotating sphere flows. *Journal of Fluid Mechanics*, 942, 2022.

[18] Javier Sierra-Ausin, Paul Bonnefis, Antonia Tirri, David Fabre, and Jacques Magnaudet. Dynamics of a gas bubble in a straining flow: Deformation, oscillations, self-propulsion. *Physical Review Fluids*, 7(11):113603, 2022.

[19] Javier Sierra-Ausin, Vincenzo Citro, Flavio Giannetti, and David Fabre. Efficient computation of time-periodic compressible flows with spectral techniques. *Computer Methods in Applied Mechanics and Engineering*, 393:114736, 2022.

[20] Sierra-Ausin, Javier, Vincenzo Citro, and David Fabre. On boundary conditions for compressible flow simulations. pages 335–340, 2019.

[21] Sierra-Ausin, Javier, Pierre Jolivet, Filippo Giannetti, and Vincenzo Citro. Adjoint-based sensitivity analysis of periodic orbits by the fourier–galerkin method. *Journal of Computational Physics*, 440:110403, 2021.

[22] Antonia Tirri, Alessandro Nitti, Javier Sierra-Ausin, Flavio Giannetti, and Marco D de Tullio. Linear stability analysis of fluid–structure interaction problems with an immersed boundary method. *Journal of Fluids and Structures*, 117:103830, 2023.

[23] Charles HK Williamson, R Govardhan, et al. Vortex-induced vibrations. *Annual review of fluid mechanics*, 36(1):413–455, 2004.